INSTITUTE FOR NUCLEAR STUDY
UNIVERSITY OF TOKYO
Tanashi, Tokyo 188
Japan

INS-Rep.-596
July 1986

SCATTERING OF POLARIZED ^{7}Li BY ^{120}Sn AND PROJECTILE-TARGET SPIN-DEPENDENT INTERACTIONS

Y. Sakuragi M. Yahiro M. Kamimura
and
M. Tanifuji

INS-Rep.-596
July 1986

SCATTERING OF POLARIZED ^{7}Li BY ^{120}Sn

AND PROJECTILE-TARGET SPIN-DEPENDENT INTERACTIONS

Y. Sakuragi
Institute for Nuclear Study, University of Tokyo, Tanashi, Tokyo, Japan

M. Yahiro
Shimonoseki University of Fisheries, Shimonoseki, Japan

M. Kamimura
Department of Physics, Kyushu University, Fukuoka, Japan

M. Tanifuji
Department of Physics and Research Center of Ion Beam Technology,
Hosei University, Tokyo, Japan

Abstract: Scattering of ^{7}Li by ^{120}Sn targets at E_{lab} = 44 MeV is investigated in the coupled-channel frame by taking account of the projectile virtual excitations to the lowest three excited states. Calculations are performed by the cluster-folding (CF) interactions and the double-folding (DF) one. Both interactions reproduce very well the expeimental data on the cross section, the vector analyzing power, the second-rank tensor ones and the third-rank tensor one in elastic and projectile inelastic scattering, although some differences are found between the CF results and the DF ones. In the calculation, the virtual excitations of the projectile are important for most of the analyzing powers and the spin-orbit interaction is indispensable for the vector analyzing power. These features are in contrast to those in ^{7}Li-^{58}Ni scattering at 20 MeV and are interpreted as over-Coulomb-barrier effects. The scattering amplitudes and the analyzing powers are investigated by the invariant amplitude method, which provides a key connecting the spin-dependent interactions to the analyzing powers. The method proposes an important relationship between the tensor analyzing powers, which is useful in analyses of both theoretical and experimental results. Finally, it is found that in the elastic scattering the second-rank tensor analyzing powers are proportional to the strength of the second-rank tensor interaction and the

vector and third-rank tensor analyzing powers to the square or cube of the strength of this interaction, while in the inelastic scattering the cross section is proportional to the square of the strength of the tensor interaction, other quantities being weakly dependent on the strength.

1. Introduction

In recent years, a lot of investigations both experimental[1-5]) and theoretical[6-17]) have been concentrated on scattering of polarized ^{6}Li and ^{7}Li by nuclei. They have clarified that analyzing power data from the polarized beam are the valuable source of the knowledge of spin-dependent interactions between nuclei. Among various theoretical approach, the coupled-channel (CC) studies with folding models of projectile-target interactions[9-12,14,16]) have provided a successful understanding of the experimental data of cross sections and vector and second-rank tensor analyzing powers for both of elastic and projectile inelastic scattering. Let us neglect excitations of the target nucleus for simplicity. The folding interaction calculated for the ground state of the projectile gives a diagonal potential for projectile-target relative motions, while the calculated between the ground state and the excited one of the projectile generates excitations of the projectile by the target[12]). The CC analyses stated above have revealed an interesting feature of the interaction; i.e. virtual excitations of the projectile caused by the folding non-diagonal interactions give rise effective spin-dependent interactions and produce some important contributions to the analyzing powers. Effects of such projectile excitations compete with those of the above diagonal potential and their resultant contributions to the analyzing powers

seem to depend largely on the relative magnitude of the incident energy to the Coulomb-barrier height[16].

At incident energies less than or comparable to the Coulomb-barrier, for example at 20 MeV or below on ^{58}Ni targets, most of the vector analyzing power of elastic scattering are explained by effective spin-orbit interactions from both of the projectile virtual excitations and higher orders of the ground-state tensor potential, while the tensor analyzing powers in the same scattering are mainly explained by the tensor potential itself[12] and the virtual-excitation effects are very small, although a small but important contribution from projectile virtual breakup processes is found in the tensor analyzing powers[18]. In this case the spin-orbit potential obtained by the folding has little effects in both the analyzing powers throughout the analyses. On the other hand, in scattering of ^{7}Li by ^{12}C at 21 MeV, the Coulomb barrier is much lower than the incident energy as is shown in fig. 1, and the spin-dependent interactions produce more complicated effects than in the scattering by the ^{58}Ni target. The folding spin-orbit potential reproduces almost the observed vector analyzing powers when the projectile excitations are switched off and it seems as if the calculation would succeed in explaining of the experimental data. However, when they are switched on once, the spin-orbit potential hardly contributes to the analyzing power and the observed analyzing power is attributed to the alternative source, i.e. the effective spin-orbit interactions from the projectile virtual excitations and the higher orders of the tensor potential which are similar to those in the ^{58}Ni case[19,20]. The tensor analyzing powers in the ^{12}C target are remarkably affected by the projectile excitations[16] contrary to the case of the ^{58}Ni target[12]. Even considering the speciality of the ^{12}C nucleus, for example the extremely large deformation[16], it may still be a plausible speculation that at incident energies higher than the Coulomb barrier details of interactions and reaction mechanisms concerned are effectively reflected in

the calculated observables and as the result the role of each spin-dependent interaction is generally different from that at energies comparable to or below the barrier. In fact, the calculated cross section and analyzing powers for the ^{12}C target become similar to those for the ^{58}Ni target with increasing the barrier height by the artificial increase of the atomic number[16]) from 6 to 15. This suggests the importance of the relative magnitude of the incident energy to the Coulomb barrier. From such consideration, it will be worthwhile to investigate in more detail the role of the various spin-dependent interactions in other cases of higher incident energies.

As the folding interaction discussed above, the following two kinds have been employed so far, i.e. the cluster-folding (CF) interaction[9-12,14]) and the double-folding (DF) one[16,21]). In the former, the projectile, say ^{7}Li, is assumed to consist of an α-particle and a triton and α-target and triton-target optical potentials are folded into the relevant states of ^{7}Li, while, in the latter, an inter-nucleon potential between a projectile nucleon and a target one is folded into the relevant states of the projectile and target. More details for the former are referred to ref. 12 and those for the latter will be described in sec. 2. Both calculations produce spin-dependent interactions of various tensor rank; for example in the CF calculation[12]), they are the central and spin-orbit potentials and the tensor interaction, the maximum rank of which is seven when the highest spin of projectile is $7/2^{-}$. The calculated cross sections and the vector and second-rank tensor analyzing powers by the CF and DF interactions are quite similar to each other in the ^{7}Li-^{58}Ni scattering at 20 MeV, as will be shown later. In the ^{7}Li-^{12}C scattering, however, they have given very different results for the above observables, particularly at large angles[16]). Such a difference between the ^{58}Ni target and the ^{12}C one will be interpreted as an effect similar to that discussed already, i.e. at higher energies than the Coulomb barrier, the details of the interaction affect the calculated quantities which allow us to

see the difference between the above two kinds of interactions. This stimulates investigations of ^{6}Li and ^{7}Li scattering at higher incident energies. Further, both of the CF and DF interactions are of phenomenological nature as will be discussed later in more detail and the theoretical justification is rather weak, in particular for their imaginary parts[12]. Thus the investigations will play a role of the validity test for such treatments of inter-nucleus interactions.

Recently, experiments have been done for scattering of polarized ^{7}Li by ^{120}Sn at 44 MeV[5]. This scattering is one of the examples where the incident energy highly exceeds the Coulomb barrier as is seen in fig.1. Furthermore, they include measurements of a third-rank tensor analyzing power. The theoretical analysis of this quantity is very interesting because they are the first experimental observation. Including of this quantity in the analysis will impose an additional examination on the theoretical models for the interaction and the reaction mechanisms concerned. In these circumstances, this paper investigates the ^{7}Li-^{120}Sn scattering theoretically, on the basis of the folding models, including the projectile virtual excitations by the coupled-channel method. In the next section, we will describe the general treatment of the projectile-target interaction by the double-folding model and compare the numerical result with the CF one[12] on scattering of ^{6}Li and ^{7}Li by ^{58}Ni at 20 MeV. This provides the validity of the use of the DF interaction by the magnificient success in explaining the data on one hand and on the other hand confirms that the CF and DF interactions give similar results for scattering of these ions at energies comparable to the Coulomb barrier. In sec. 3, the roles of the folding potentials and the effective interactions due to the virtual excitations are studied by both of the CF and DF interactions for the ^{7}Li-^{120}Sn scattering. The results of these calculations are compared with each other and also compared with the experimental data. There some considerable differences are found between the

two kinds of calculations, the origin of which is investigated through the form factors of the interactions. In both cases, however, the agreement between the theory and the experiment is quite successful within the experimental errors, including the third-rank tensor analyzing power. In sec. 4, the results of the calculation are analyzed by the invariant amplitude method[22]). This gives the deeper insight of the effects of the spin-dependent interactions; for example, it clarifies the reason why the vector and third-rank tensor analyzing powers are particularly influenced by the choice of the interaction or by the reaction mechanism. The method also proposes an important relationship between the tensor analyzing powers, which is useful in analyses of both theoretical results and experimental data. Finally, the dependences of the cross sections and analyzing powers on the strength of the second-rank tensor interactions are investigated. Roughly speaking, the interactions contribute to the second-rank tensor analyzing powers in the first order and to the vector and third-rank tensor analyzing powers in the second or third order in the elastic scattering, while the cross section in the inelastic scattering is affected by this interaction in the second order. Sec. 5 will be devoted to the summary and discussions of the results.

2. Double-folding interactions and tests of its validity in scattering of ^{6}Li and ^{7}Li by ^{58}Ni at 20 MeV

The double-folding (DF) interaction between two nuclei have been discussed earlier in detail[23]). In this section, the essence of the method is summarized and its validity is examined by comparing the numerical result with the CF calculation and also with the experimental data in the ^{6}Li-^{58}Ni and ^{7}Li-^{58}Ni scattering at 20 MeV. Let us consider an interaction V_{ji} for the excitation of the projectile P from the i-th state to the j-th state, while

the target nucleus T is in the ground state. As a special case, this interaction gives the potential for the projectile-target relative motion when both of the i-th and j-th states are the ground state. The DF method gives

$$V_{ji}(R)=(1+iN_I)\int\rho_{Pji}(r_1)\rho_{T00}(r_2)v_{NN}(r_1+R-r_2)d\,r_1 d\,r_2\ , \qquad (2.1)$$

where the coordinates r_1, r_2 and R are shown in fig. 2, ρ_{Pji} is the transition nucleon density of P from the i-th state to the j-th state and ρ_{T00} is the ground state nucleon density of the target nucleus. The quantity v_{NN} is the inter-nucleon potential which is taken to be the so-called M3Y interaction modified with knock-on-type exchange effects[24]. In order to introduce an absorption effect, the imaginary part with the factor iN_I and the same shape as the real one is added to this interaction, where N_I is a flexible parameter and is fixed by fitting the calculated elastic-scattering cross section to the measured. Such a treatment has been successful in high energy scattering[23,25].

The density ρ_{Pji} is calculated by microscopic wave functions $\Psi_i(P)$. For the ^{7}Li projectile, for example,

$$\rho_{Pji}(r_1) = \langle\Psi_j(^7\mathrm{Li})|\sum_{n=1}^{7}\delta(r_1-r_n')|\Psi_i(^7\mathrm{Li})\rangle\ . \qquad (2.2)$$

The wave function $\Psi_i(^7$Li) is obtained by a microscopic treatment[16,23] of the α-t cluster model, which takes account of the antisymmetrization between seven nucleons and reproduces the data of the binding energy and the quadrupole moment for the ground state[26], those of the excitation energy and B(E2) for the first excited state and α-t phase shifts[27] for the scattering states. The density thus obtained is good descriptions of form factors of electron elastic and inelastic scattering[28]. For ρ_{T00}, the nucleon density obtained from the electron-scattering data[29] with the correction due to the proton

charge distribution is employed. In the numerical calculation of V_{ji}, spin-orbit interactions are neglected for simplicity, the effect of which will be discussed later.

The coupled-channel calculation for the ^{7}Li-^{58}Ni scattering is carried out by taking account of the $1/2^-_1$, $7/2^-_1$ and $5/2^-_1$ excited states in addition to the ground state of $3/2^-$ for ^{7}Li with N_I=0.7. The results for the cross section and the vector and tensor analyzing powers are compared with those by the CF interaction[12]) and also with the data[3]) in fig. 3a for the elastic scattering and in fig. 3b for the inelastic scattering leading to the first excited state of ^{7}Li. In the figures the CF calculation includes the spin-orbit potential but it does not yield any real effect. Except for several minor differences the results by the DF calculation are quite similar to those by the CF calculation and fit the experimental data very well. Similar DF calculations with the same N_I are performed for the ^{6}Li-^{58}Ni scattering where the 1^+ ground state and the 3^+_1, 2^+_1 and 1^+_2 excited states and non-resonant breakup states of 1^+(s), 0^-, 1^- and 2^- are considered by the coupled-channel method. The calculated cross section and vector analyzing power in the elastic scattering are in good agreements with those by the CF calculation[12]) which reproduces the experimental data[30]) very well. These analyses provide the validity for the use of the DF interaction. In the next section, we will examine the DF interaction as well as the CF one in scattering at a higher incident energy.

3. ^{7}Li-^{120}Sn scattering by the CF and DF interactions

The scattering of ^{7}Li by ^{120}Sn at 44 MeV will be analyzed in the following by the cluster-folding (CF) interaction and also by the double-folding (DF) one. The low excited states of ^{7}Li of $1/2^-$, $7/2^-$ and $5/2^-$ are

taken into account in addition to the ground state of $3/2^-$, in the coupled-channel framework. In the calculation of the CF interaction, several combinations of the α-^{120}Sn and t-^{120}Sn optical potentials are examined, the numerical values of potential parameters being in table 1. The combination used as the standard is set A1 for the α-^{120}Sn potential[†31)] and set T1 for

---

[†]The mass number of Sn is not specified in the reference for A1 and A2 but the potentials are assumed to be valid for ^{120}Sn because ^{120}Sn has the largest abundance in the natural tin and the potential parameters depend weakly on the target mass number for this element.

---

the t-^{120}Sn one[31)], where the latter does not include the spin-orbit (LS) part. In the DF calculation, the nucleon density of ^{120}Sn is obtained from the electron-scattering data[32)] and N_I is determined so as to fit the cross-section data of the ^{7}Li elastic scattering, resulting $N_I = 0.17$. The investigated is the cross section σ, the vector analyzing power iT_{11}, the second-rank tensor analyzing powers $^TT_{20}$, T_{20} and T_{21} and the third-rank tensor analyzing power $^TT_{30}$ in the elastic scattering and in the inelastic one leading to the first excited state of ^{7}Li ($1/2^-$, 0.48 MeV).

The results of the CF calculation and those of the DF one are compared with each other and also with the experimental data[33)] in fig. 4. The gross behaviour of the above observables in their angular distributions are quite similar between the two calculations and both calculations reproduce the data very well within their experimental errors. These results justify the underlying theoretical frame. There several minor differences are found between the two calculations. The DF cross section is slightly larger than the CF one giving better agreement with the measured in both elastic and inelastic scattering. For the analyzing powers, the calculated by the DF interaction oscillates more strongly in the angular distribution than that by

the CF one and is consistent with the angular fluctuations of the data. From the cross sections and such fine structures in the analyzing powers, the DF calculation looks better than the CF one in the agreement with the data but the definite superiority of the DF interaction is hardly identified in the present experimental accuracy. It should be emphasized that the calculated $^{T}T_{30}$ reproduces well the characteristic feature of the measured one in both elastic and inelastic scattering. This provides the guarantee of the validity for the present theoretical assumptions.

In the CF calculation, a deeper α-Sn potential[31]) A2 is examined but the difference of the calculated between A1 and A2 is very small; for example, the results by the combination of A2 and T1 are not distinguishable from those by the combination of A1 and T1 in most observables. Since the LS potential has not been derived for the triton scattering from ^{120}Sn in the present energy region, we will refer the optical potential from ^{116}Sn, T2 which includes the LS part, as an alternative of the triton potential[34]). The use of this triton potential will help us in studying effects of the LS potential in the ^{7}Li-^{120}Sn scattering. In fig. 5, the following two combinations are compared with each other and also with the experimental data; i.e. the combination of A1 and T2 and that of A1 and T3 where T3 is the same as T2 except for the neglect of the LS part. The results of these combinations are generally similar to those from the standard combination of A1 and T1, with a few exceptions for example the elastic vector analyzing power, and are still good descriptions of the experimental data. In the vector analyzing power of the elastic scattering, a remarkable effect of the LS interaction is observed by comparing set T2 to set T3; i.e., the magnitude of iT_{11} suffers from a big reduction due to this interaction. This LS effect is demonstrated in fig. 6, where the pure effect of this interaction is displayed by neglecting the tensor interaction and thus the coupling with the ^{7}Li excited states, the input potentials being the combination of A1 and T2. The LS interaction

itself gives positive vector analyzing power in most angles which has the opposite sign to the contribution from the tensor interaction. The final vector analyzing power is the result of the competition between the LS interaction and the tensor interaction accompanied by the projectile virtual excitation. Such an important contribution of the LS interaction is a typical feature of the scattering at energies over the Coulomb barrier and has not been observed in ^{6,7}Li-^{58}Ni scattering at 20 MeV. More details, which include similar effects in ^{7}Li-^{12}C scattering, will be given in ref. 20. Further, rather minor effects of the LS interaction appear in elastic $^{T}T_{20}$, T_{21}, $^{T}T_{30}$ and inelastic iT_{11} in fig. 5. Such LS effects are seen in comparison betwee. the combination of A1 and T1 and that of A1 and T4 where the LS part of T2 is added to T1. Other combinations which include A2 as well as A1 are studied. Through these investigations, a tendency is found, i.e. the vector analyzing power and the third-rank tensor analyzing power in the elastic scattering are particularly easy to be affected by changes of the input optical potentials, whether the LS interaction is included or not. This will be related to the fact that in these analyzing powers the tensor interaction acts only in its second order or higher orders, which will be discussed later in more detail. The analysis also reveals that the calculated analyzing powers are more sensitive to the triton central potential than to the alpha-particle one. This is because in the folding interactions the contribution of the former potential has larger magnitudes than that of the latter at the nuclear surface region.

To clarify the origin of the differences between the CF result and the DF one, the form factors of the central interaction in the elastic-scattering channel, for example, are investigated in the region where the interactions produce large contributions to the scattering amplitude. In the case of strong absorption like heavy-ion scattering by nuclei, the characteristic feature of the scattering is mainly governed by interactions at the strong

absorption radius R_s which is assumed to be determined by the quarter-point recipe[35]),

$$R_s = \frac{\eta}{k}\left(1 + \mathrm{cosec}\left(\frac{1}{2}\theta_{1/4}\right)\right) , \tag{3.1}$$

where η is the so-called Sommerfeld parameter

$$\eta = \frac{ZZ'e^2}{\hbar v} . \tag{3.2}$$

The quantity $\theta_{1/4}$ is defined for the Fresnel-type diffraction scattering so that the cross section falls to one quarter of the Rutherford value at $\theta = \theta_{1/4}$. Fig. 7 shows the form factors of the real part and those of the imaginary one in the region of 5 - 14 fm of the ^{7}Li-^{120}Sn relative distance. The figure contains two kinds of the CF interactions, the combination of A1 and T1 and that of A2 and T1, and the DF interaction. The absorption radius is 10.6 fm in the present case. Around this point, the two CF form factors are very similar with each other while the DF form factor is much smaller than the CF ones for both real and imaginary parts. Such differences of form factors between the interactions will explain why the two CF interactions give the similar results but the DF interaction gives the different ones. More details will be discussed in the next section in terms of the invariant amplitudes.

Details of the projectile-excitation effects are shown in fig. 8 for the standard CF calculation, where the calculations by the single channel ($3/2^-$), the two channels ($3/2^-$, $1/2^-$), the three channels ($3/2^-$, $1/2^-$, $7/2^-$) and the four channels ($3/2^-$, $1/2^-$, $7/2^-$, $5/2^-$) are displayed separately, where the single-channel calculation is only for the elastic scattering. Generally speaking, the effects of the projectile virtual excitations are large for the elastic-scattering observables, particularly for iT_{11} and $^{T}T_{30}$. In most observables investigated, the contribution of the $5/2^-$ state is not

negligible, which was very small in the case of the ^{7}Li-^{58}Ni scattering at 20 MeV[12]). Similar effects of the projectile virtual excitations are observed in the DF calculation where the effects are much more pronounced. Finally, it is remarked that the projectile excitations by Coulomb interaction produces important contribution to most observables, particularly to the cross section, the vector analyzing power and the third-rank tensor analyzing power in the inelastic scattering. In this section, we have found several features of the calculated analyzing powers which have not been seen in the previous analyses of the ^{7}Li-^{58}Ni scattering. These new features will be considered as the reflection of the fact that the incident energy is much higher than the Coulomb barrier.

4. Analyses by the invariant amplitudes method

It has been discussed that the invariant amplitude method[22]) is useful in analyses of polarization phenomena in nuclear reactions because it provides a guide-post for solving complicated effects of many kinds of spin-dependent interactions[6,12,22,36]). The method is based on the expansion of the transition amplitude in accordance with the tensor rank in the spin space. In this sense, the method resembles the theory for deuteron scattering published later[37]). However, the invariant amplitude method uses explicitly the associated space tensors which are helpful in practical use. Also it has been developed in more general form and thus it is applicable to any two-body reaction. In the present section, we will apply the method to the ^{7}Li-^{120}Sn scattering to clarify the structure of the scattering amplitude in the spin space and discuss how the spin-dependent interactions govern the analyzing powers.

4.1 The invariant amplitudes in elastic scattering of ^{7}Li

First, we will describe the outline of the theory. The transition matrix M can be expanded in terms of the tensor in the spin space $\mathcal{S}_{k\kappa}$,

$$M = \sum_{k\kappa} (-)^{\kappa} \mathcal{S}_{k-\kappa} \mathcal{R}_{k\kappa} , \tag{4.1}$$

where $\mathcal{R}_{k\kappa}$ is the associated ordinary space tensor and its matrix element can be described by the tensor of the same rank constructed from $\mathbf{k}_i$ and $\mathbf{k}_f$, the initial and final momenta. In the case where the spin of the target nucleus and that of the residual one are zero and no parity change happens in the transition, the matrix element of M is given by[22],

$$\langle s_f, \nu_f; \mathbf{k}_f | M | s_i, \nu_i; \mathbf{k}_i \rangle$$

$$= (-)^{s_f - \nu_f} \sum_k (s_i s_f \nu_i - \nu_f | k\kappa) \sum_{r=\bar{k}-k}^{k} [C_r(\Omega_i) \times C_{\bar{k}-r}(\Omega_f)]_{\kappa}^{k} F_{kr} , \tag{4.2}$$

where Ω_i and Ω_f are the solid angles of $\mathbf{k}_i$ and $\mathbf{k}_f$, respectively, $s_i(\nu_i)$ and s_f (ν_f) are the spin (z-component) of the incident particle and the emitted one, respectively, and $\bar{k}$ is k for k = even and k+1 for k = odd. The quantity $C_{\ell m}(\Omega)$ is related to the spherical harmonics $Y_{\ell m}(\Omega)$ as

$$C_{\ell m}(\Omega) = \sqrt{\frac{4\pi}{2\ell+1}}\, Y_{\ell m}(\Omega) .$$

The Clebsch-Gordan coefficient $(s_i s_f \nu_i - \nu_f | k\kappa)$ arises from the matrix element of $\mathcal{S}_{k-\kappa}$ and the factor constructed from C_r and $C_{\bar{k}-r}$ describes that of $\mathcal{R}_{k\kappa}$. Other trivial factors like the physical part of the matrix element of $\mathcal{S}_{k-\kappa}$ are included in F_{kr}. The amplitude F_{kr} is invariant under rotations of the coordinate axes and is a function of θ, the angle between $\mathbf{k}_i$ and $\mathbf{k}_f$, the c.m.

energy and the Q-value. The invariant amplitude F_{kr} is designated by the rank of the spin tensor, with which F_{kr} is associated; for example, F_{00}, F_{11} and F_{2r} $(r = 0,1,2)$ are the scalar, vector and second-rank tensor terms, respectively. In the first order of interactions, F_{00}, F_{11} and F_{2r} represent the contributions to the scattering amplitudes from the central, spin-orbit and second-rank tensor interactions, respectively. In principle, they contain any higher-order contribution of these interactions within the restriction due to their tensorial properties.

In the case of the elastic scattering of ^{7}Li, the matrix element of M is represented by designating the row and column by the z-component of the ^{7}Li spin as[6]

$$M = \begin{pmatrix} A & B & C & D \\ E & F & G & H \\ H & -G & F & -E \\ -D & C & -B & A \end{pmatrix} , \tag{4.3}$$

where A-H satisfy the elastic-scattering conditions due to the time-reversal theorem

$$(C+H) = \sqrt{3}\,(A-F) - 2(B+E)\cot\theta \tag{4.4}$$

and

$$(B-E) = \sqrt{3}\,(G+D) + 2(C-H)\cot\theta\ . \tag{4.5}$$

Each matrix element of (4.3) is rewritten in terms of the invariant amplitudes $F_{k\kappa}$ by the use of (4.2), which will be given later. The elastic-scattering conditions become

$$F_{22} = F_{20} \tag{4.6}$$

and

$$F_{33} = F_{31} \ . \tag{4.7}$$

Thus we have one scalar, one vector, two second-rank tensor and two third-rank tensor amplitudes as independent ones, which can be chosen in the reference frame, $y /\!/ k_i \times k_f$ and $z /\!/ k_i$, as

$$U \equiv F_{00} \ , \tag{4.8}$$

$$S \equiv \sqrt{\frac{5}{8}}\, F_{11} \sin\theta \ ,$$

$$T_{2\alpha} \equiv \frac{1}{2} F_{20}(3\cos^2\theta+1) + \sqrt{\frac{2}{3}}\, F_{21} \cos\theta \ ,$$

$$T_{2\beta} \equiv \sqrt{\frac{3}{4}}\, F_{20} \sin^2\theta \ ,$$

$$T_{3\alpha} \equiv \sqrt{\frac{5}{4}}\, F_{31} \sin^2\theta \cos\theta + \sqrt{\frac{3}{8}}\, F_{32} \sin^2\theta \ ,$$

$$T_{3\beta} \equiv \sqrt{\frac{15}{64}}\, F_{31} \sin^3\theta .$$

The amplitude U is related to the scalar, S to the vector, $T_{2\alpha}$ and $T_{2\beta}$ to the second-rank tensor and $T_{3\alpha}$ and $T_{3\beta}$ to the third-rank tensor in the spin space, respectively. With these new amplitudes, A-H are given by

$$A = \frac{1}{2}(U + T_{2\alpha}) \ , \tag{4.9}$$

$$B = \frac{1}{4}(\sqrt{3}T_{2\alpha} - T_{2\beta})\tan\theta + \frac{\sqrt{3}}{5}(S + T_{3\beta}) + \frac{2}{5} T_{3\alpha} \cot\theta \ ,$$

$$C = \frac{1}{2}(T_{2\beta} + T_{3\alpha}) \ ,$$

$$D = T_{3\beta} \ ,$$

$$E = \frac{1}{4}(\sqrt{3}T_{2\alpha} - T_{2\beta})\tan\theta - \frac{\sqrt{3}}{5}(S + T_{3\beta}) - \frac{2}{5}T_{3\alpha}\cot\theta ,$$

$$F = \frac{1}{2}(U - T_{2\alpha}) ,$$

$$G = \frac{2}{5}S - \frac{2\sqrt{3}}{5}T_{3\alpha}\cot\theta - \frac{3}{5}T_{3\beta}$$

and

$$H = \frac{1}{2}(T_{2\beta} - T_{3\alpha}) .$$

Similar theoretical developments for the inelastic scattering are given in Appendix.

Since the analyzing powers are described by A-H, they can be expressed by $U \sim T_{3\beta}$. The expressions are the key for connecting the spin-dependent interactions to the polarization quantities, which will be discussed in the next subsection. The amplitudes U, S, $T_{2\alpha}$ ($T_{2\beta}$) and $T_{3\alpha}$ ($T_{3\beta}$) are the representative of the central, spin-orbit, second-rank tensor and third-rank tensor interactions, respectively, in their first order and thus it is reasonably speculated that U is dominant and other amplitudes are comparatively small because the central interaction is strong and the spin-dependent interactions are weak. The numerical calculations show that the order of magnitude of these amplitudes is approximately described by

$$|U| > |S| \approx |T_{2\alpha}| \approx |T_{2\beta}| > |T_{3\alpha}| \approx |T_{3\beta}| \qquad (4.10)$$

at most angles for both the CF and DF interactions, where the left-hand side of the inequality sign is larger than the right-hand side by almost one order of magnitude. The magnitude of these amplitudes are shown in fig. 9, for example for the CF interactions of the A1-T2 and A1-T3 combinations, where the effect of the LS potential and that of the projectile virtual excitations are

also examined. The figure shows that the above relation, (4.10) holds independently of the presence of the LS potential or the projectile virtual excitations. As is seen in the figure, $|S|$, $|T_{3\alpha}|$ and $|T_{3\beta}|$ are affected considerably by the presence of the LS interaction or by the projectile virtual excitations, while other amplitudes are affected very little. In more detail, the projectile excitation increases $|S|$ by a large amount but decreases $|T_{3\alpha}|$ and $|T_{3\beta}|$ seriously and the LS potential affects these amplitudes in a quite opposite way with less amount. This will be discussed later in connection with the calculated analyzing powers. The amplitudes calculated by the deep CF interaction are almost equivalent to those by the shallow interaction. The effects of the projectile excitations in the DF calculation are similar to those in the CF one; i.e. only $|S|$, $|T_{3\alpha}|$ and $|T_{3\beta}|$ receive serious effects. Fig. 10 compares $|U|$-$|T_{3\beta}|$ between the CF calculation and the DF one, where the combination A1-T1 is used for the CF calculation, corresponding to fig. 4. Differences between the two calculations are found in all amplitudes, which produce the differences in the calculated quantities in fig. 4. Referring to the expressions of ${}^{T}T_{20}$, T_{20} and T_{21} in the following subsection, one will understand that the oscillatory angular dependence of $|T_{2\alpha}|$ in the DF calculation in fig. 10 is reflected in that of the second-rank tensor analyzing powers in fig. 4. Rather large CF-DF differences are observed in $|S|$, $|T_{3\alpha}|$ and $|T_{3\beta}|$. This is consistent with the theoretical observation in elastic iT_{11} and ${}^{T}T_{30}$ in fig. 4.

In the absence of the LS interaction, the main spin-dependent interaction is the second-rank tensor one because the parity of the folding interaction is even and the fourth- and sixth-tensor interactions are comparatively weak. In this case, the amplitudes S, $T_{3\alpha}$ and $T_{3\beta}$ will arise from the second order or higher orders of the second-rank tensor interactions. Thus it is interesting to examine how the amplitudes U-$T_{3\beta}$ are governed by these interactions. In fig. 11, the magnitudes of U-$T_{3\beta}$ obtained by reducing the strength of the

second-rank tensor part of the CF interactions to one half of the original one are compared with those by the original interactions, where the higher-rank tensor interactions in addition to the spin-orbit interaction are neglected to simplify the consideration. The calculation is based on the A1-T3 combination and is performed in the four-channel frame. In the figure, the magnitudes of $T_{2\alpha}$ and $T_{2\beta}$ are decreased by about one half and those of S, $T_{3\alpha}$ and $T_{3\beta}$ by about a quarter by the reduction of the tensor interactions, while U is scarcely changed. This means that $T_{2\alpha}$ and $T_{2\beta}$ are proportional to the strength of the second-rank tensor interaction and S, $T_{3\alpha}$ and $T_{3\beta}$ are proportional to the square of the strength of that interaction. When the higher-rank tensor interactions are taken into account, such proportionalities are modified but the modifications are very small except for $T_{3\alpha}$ and $T_{3\beta}$ at small angles, as is shown in the figure. These features can be understood by assuming that $T_{2\alpha}$ and $T_{2\beta}$ are mainly produced by the first order of the second-rank tensor interactions, while S, $T_{3\alpha}$ and $T_{3\beta}$ are produced essentially by the second order of that interaction. The amplitude U is dominantly governed by the central interaction and is almost independent of the tensor one. Thus, in the present scattering, the amplitudes S-$T_{3\beta}$ are good measure of the second-rank tensor interactions.

4.2 Invariant amplitude analyses of the analyzing powers

Considering (4.10), one can neglect in a good approximation the terms which include $T_{3\alpha}$ and $T_{3\beta}$ but not U in describing the elastic scattering analyzing powers by U etc.. These approximate formulae are given in the following, the full expressions being in Appendix.

$$iT_{11} = \frac{2\sqrt{6}}{\sqrt{5}N}\,\mathrm{Im}\left\{\frac{1}{\sqrt{3}}US^{*} + \frac{2}{5\sqrt{3}}ST_{2\alpha}^{*} + \frac{2}{5}ST_{2\beta}^{*}\right\}, \qquad (4.11)$$

$$T_{20} = \frac{2}{N}\,\mathrm{Re}\{UT_{2\alpha}^{*} - \frac{4}{25}|S|^{2} - \frac{3}{5}ST_{2\alpha}^{*}\tan\theta + \frac{\sqrt{3}}{5}ST_{2\beta}^{*}\tan\theta\}\ ,$$

$$T_{21} = \frac{2\sqrt{2}}{N}\,\mathrm{Re}\{-\frac{\sqrt{3}}{4}UT_{2\alpha}^{*}\tan\theta + \frac{1}{4}UT_{2\beta}^{*}\tan\theta - \frac{\sqrt{3}}{5}ST_{2\alpha}^{*} + \frac{1}{5}ST_{2\beta}^{*}\}\ ,$$

$$^{T}T_{20} = -\frac{1}{N}\,\mathrm{Re}\{UT_{2\alpha}^{*} + \sqrt{3}UT_{2\beta}^{*} - \frac{16}{25}|S|^{2}\}$$

and

$$^{T}T_{30} = \frac{1}{\sqrt{5}N}\,\mathrm{Im}\{-2\sqrt{3}UT_{3\alpha}^{*}\cot\theta - 8UT_{3\beta}^{*} + \frac{6}{5}ST_{2\alpha}^{*} + \frac{6\sqrt{3}}{5}ST_{2\beta}^{*}\}\ ,$$

with

$$N = 4_{0}\ .$$

To investigate the validity of the approximation, three kinds of calculation for the analyzing powers are displayed in fig. 12; the calculations by the exact formulae, those by eq. (4.11) (approximation I) and the calculations by neglecting the U-independent terms except for N (approximation II). All calculations are performed in the four-channel CC frame and the interaction used is the CF one of A1+T2. In the figure, it is clear that eq. (4.11) is very accurate for T_{20}, T_{21} and $^{T}T_{20}$ and is quite close to the exact calculation in iT_{11} and $^{T}T_{30}$, while the neglect of the U-independent terms (approximation II) has high validity for the second-rank tensor analyzing powers but not for iT_{11} and $^{T}T_{30}$. These features are also found in the calculations by various combinations of the alpha potential and the triton one and in the DF calculation. It should be noted that the calculated $^{T}T_{30}$ changes its sign by including the terms of $ST_{2\alpha}^{*}$ and $ST_{2\beta}^{*}$. This happens due to the virtual-excitation effect as is shown in the following. In the comparison

of the four-channel calculations with the single-channel ones in fig. 12, the sign of $^{T}T_{30}$ by the approximation II is changed by the projectile virtual excitation. Further,as is seen in fig. 9, the amplitudes $|T_{3\alpha}|$ and $|T_{3\beta}|$ are decreased seriously by increasing the coupled channels from one to four, while $|S|$ is increased by this increase of the channels. This decrease of $|T_{3\alpha}|$ and $|T_{3\beta}|$ reduces the magnitude of contributions of the U-dependent terms to $^{T}T_{30}$ as is seen in fig. 12 (approximation II) and the increase of $|S|$ increases the relative importance of the terms $ST^{*}_{2\alpha}$ and $ST^{*}_{2\beta}$. These effects cause the competition between the U-dependent terms and U-independent ones in $^{T}T_{30}$ of eq. (4.11), resulting the final change of sign in $^{T}T_{30}$.

Since the second-rank tensor analyzing powers are described well by only the U-dependent terms, one can derive the following formula by neglecting U-independent terms,

$$^{T}T_{20} = -2T_{20} - \sqrt{6}T_{21}\cot\theta \tag{4.12}$$

or

$$T_{22}\sin\theta = \sqrt{\frac{3}{2}}\,T_{20}\sin\theta + 2T_{21}\cos\theta \tag{4.13}$$

with

$$^{T}T_{20} \equiv -\frac{1}{2}(T_{20} + \sqrt{6}T_{22}) \ .$$

In fig. 13, $^{T}T_{20}$ obtained by eq. (4.12) with T_{20} and T_{21} calculated exactly is compared to the exact $^{T}T_{20}$. The calculations are performed by the two kinds of interaction; the CF interaction of A1-T2 combination and the DF one, the virtual-excitation effects being taken into account by the four-channel coupling frame. The comparison justifies eq. (4.12) fairly well for the CF interactions. For the DF interaction, the characteristic feature of the exact calculation is reproduced by (4.12), though its right-hand side oscillates more strongly than the exact in the angular distribution. Such deviations of the approximation from the exact are related to the virtual-excitation effect

because the agreement with the exact calculation is much better in the single-channel calculations. The validity of (4.12) can also be examined in a way free from the choice of the interaction. In the ^{7}Li-^{58}Ni scattering at 20 MeV, the shape-effect formulae[3] have been found to be very good descriptions of T_{20}, T_{21} and T_{22}. The formulae have been derived semi-classically[3] and also quantum-mechanically[12]. They are for T_{20} and T_{21}

$$T_{20} = (1 - 3\sin^2\frac{\theta}{2})^{T}T_{20} \qquad (4.14)$$

and

$$T_{21} = -\sqrt{\frac{3}{2}}\sin\theta\,{}^{T}T_{20} \ . \qquad (4.15)$$

In the present case, these formulae also describe the measured T_{20} and T_{21} very well by using the measured $^{T}T_{20}$ for the right-hand side of the equations, as is shown in fig. 14. These formulae satisfy eq. (4.12) exactly, which means that the experimental data themselves satisfy eq. (4.12). Similar considerations can be applied to other scattering; for example the validity of (4.13) has been confirmed in scattering of ^{6}Li and ^{7}Li by ^{58}Ni targets at 20 MeV[36]. The relation (4.12) or (4.13) is a measure of the spin-dependent interactions; that is, when it is satisfied, effects of higher order terms of the spin-dependent interactions are small in these analyzing powers, whether the analyzing powers are the calculated or the measured. The approximation used in the derivation of (4.12) or (4.13) can be avoided by allowing the participation of more polarization quantities in the formulae. Such exact relationships will be discussed elsewhere[38].

It should be remarked that the properties of U-$T_{3\beta}$ discussed in the previous subsection are reflected in the calculated analyzing powers. This can be understood through the expressions (4.11). For example, as is discussed already, the amplitudes S, $T_{3\alpha}$ and $T_{3\beta}$ are selectively influenced by the input potentials and the reaction mechanism; particularly, $|S|$ is increased and

$|T_{3\alpha}|$ and $|T_{3\beta}|$ are decreased seriously by the virtual excitations of the projectile, while other amplitudes are almost stable. When these properties are combined with eq. (4.11) where all terms of iT_{11} and $^{T}T_{30}$ contain S, $T_{3\alpha}$ or $T_{3\beta}$, it will be reasonably understood why only iT_{11} and $^{T}T_{30}$ are easily affected by the change of interactions or by the projectile virtual excitations. In the inelastic scattering leading to the $1/2^{-}$ state of ^{7}Li, similar analyses are performed, where we have one vector and three second-rank tensor amplitudes but no scalar amplitude. The details are given in Appendix. The second-rank tensor analyzing powers are mainly governed by the corresponding tensor amplitudes, while in iT_{11} and $^{T}T_{30}$ the contributions of the above four amplitudes compete with each other. The absence of U makes the analyses more complicated.

In the previous subsection, the invariant amplitudes have been found to depend on the strength of the second-rank tensor interaction in the definite ways; $|U|$ is almost independent on the strength, $|T_{2\alpha}|$ and $|T_{2\beta}|$ are nearly proportional to the strength and $|S|$, $|T_{3\alpha}|$ and $|T_{3\beta}|$ are approximately proportional to the square of the strength. Thus it is interesting to investigate how such dependences of the amplitudes are reflected on the cross sections and analyzing powers. The calculation is carried out in the four-channel coupling frame, the input potential being the A1-T3 combination. The calculations performed by reducing the strength by one half are compared with those by the full strength, where the fourth- and sixth-rank tensor interactions are neglected. The results are shown in fig. 15. In the elastic scattering, $^{T}T_{20}$, T_{20} and T_{21} are almost proportional to the tensor interaction strength. This is easily understood by considering of the approximation II for the analyzing powers together with the properties of $|T_{2\alpha}|$ and $|T_{2\beta}|$ mentioned above. The magnitude of iT_{11} and $^{T}T_{30}$ are decreased by the reduction of the tensor strength more strongly than the square of the strength. From the behaviours of $|S|$, $|T_{3\alpha}|$ and $|T_{3\beta}|$ observed in fig. 11,

one will see that each term of iT_{11} and $^{T}T_{30}$ in eqs. (4.11) is proportional to the square or cube of the tensor interaction strength. Thus the dependence of iT_{11} and $^{T}T_{30}$ on the strength is quite reasonable. These results indicate that the second-rank tensor interactions contribute to the second-rank tensor analyzing powers mainly in the first order and to the vector and third-rank tensor analyzing powers in the second or third order in the perturbation-theoretical sense. In the inelastic scattering, the cross section is decreased to a quarter by reducing the strength of the second-rank tensor interactions by one half, while all analyzing powers are changed by small amounts. This will be explained by considering that all amplitudes in the inelastic scattering are decreased by one half or one fourth by the reduction of the tensor strength and the decreases in the amplitudes are almost cancelled between the numerator and the denominator in the analyzing powers but no cancellation is in the cross section. Because of the lack of U, the dominant contributions to the cross section come from the tensor amplitudes and they are proportional to the square of the tensor strength. From these analyses, it will be emphasized that, in the elastic scattering, the analyzing powers are the measure of the second-rank tensor interactions, while, in the inelastic scattering, the cross section is the measure of these interactions.

5. Summary and discussion

The elastic scattering and inelastic one leading to the $1/2^-$ excited state of the projectile are investigated in the ^{7}Li-^{120}Sn case by the coupled-channel method, where the $1/2^-$ bound state and the $7/2^-$ and $5/2^-$ resonance states of ^{7}Li are taken into account in addition to the $3/2^-$ ground state. Between the projectile and the target, the two kinds of interaction are

studied; the cluster folding (CF) interaction and the double-folding (DF) one. In the former, as the input the α-target and triton-target optical potentials are employed under the assumption of the α-t cluster model for ^{7}Li, where several combinations of these potentials are examined. In the DF calculation, the so-called M3Y inter-nucleon potential is folded between ^{7}Li and ^{120}Sn, the validity of the method being confirmed in ^{6,7}Li-^{58}Ni scattering in advance.

The calculation shows that both of the CF and DF interactions are quite successful in explaining the experimental data of the elastic scattering and those of the inelastic scattering simultaneously. The newly observed third-rank tensor analyzing powers are reasonably predicted by the calculation justifying the theoretical frame. Through these analyses, it is found that the difference between the interactions and the virtual excitations of the projectile affect the analyzing powers seriously which are in contrast with the case of ^{7}Li-^{58}Ni scattering at 20 MeV. Particularly, the calculated vector analyzing power is found to be given by the competition between the spin-orbit interaction and the second-rank tensor one. These will be understood as the above-Coulomb barrier effects. Here, effects of the folding LS potential are investigated for the CF calculation which uses essentially the ^{7}Li-^{116}Sn interaction because of the lack of the knowledge of the t-^{120}Sn spin-orbit potential. Since the LS potential affects substantially the vector and third-rank tensor analyzing powers, reexaminations by the CF interaction with the t-^{120}Sn spin-orbit potential are desirable to draw any definite conclusion on the real effect of the LS potential on the analyzing powers. Accordingly, the DF calculation should be improved so as to include the proper LS interaction in any way.

To get more insights of the calculation, the analyses are extended by the invariant amplitude method. The theory classifies the scattering amplitude into the scalar, vector, second-rank tensors and so on in the spin space and thus they reflect effects of the corresponding spin-dependent interactions.

For the elastic scattering, for example, it is clarified how these amplitudes are influenced by the choice of the interaction or by the reaction mechanism. In particular, the vector and third-rank tensor amplitudes are easily affected by these factors. The analyses also find that the scalar amplitude is larger than other amplitudes. This allows us to reduce the expressions of the analyzing powers into simple forms, the validity of which is confirmed numerically. In the extreme case where all U-independent terms are neglected, one can derive a relationship between the second-rank tensor analyzing powers. The relationship is justified by the CC calculation successfully for the CF interaction and satisfactorily for the DF one. The experimental data are well described by the relation formula. Thus the relationship will be useful in investigating these analyzing powers both theoretically and experimentally. The simplified forms and the properties of the amplitudes discussed above lead to understanding of the reason why the vector and the third-rank tensor analyzing powers are easily affected by the choice of the interaction or by the projectile virtual excitations.

Further, the following is found by the CC calculation. In the elastic scattering, the second-rank tensor analyzing powers are approximately proportional to the strength of the second-rank tensor interaction and the magnitudes of vector and third-rank tensor analyzing powers are varied by the change of the strength more strongly than the square of the interaction strength, the cross section being almost stable against the variation of the interaction. On the other hand, in the inelastic scattering, the cross section is proportional to the square of the second-rank tensor interaction strength but the analyzing powers are weakly dependent on the strength. Thus the analyzing powers are good measures of the second-rank tensor interactions in the elastic scattering, while the cross section is the measure in the inelastic scattering. The above consideration is of course global understanding of the feature of the tensor interaction and, in detail, the

higher orders of the second-rank tensor interaction produce important effects on the calculated quantities. In fact, as mentioned already, the projectile virtual excitations contribute considerably to the second-rank tensor analyzing powers through higher orders of the interaction in addition to the fourth- and sixth-rank tensor interactions. Since it is clarified that, above the Coulomb barrier, scattering and reactions of ^{7}Li provide useful tools of studying the interactions from the target, more investigations are desirable in such energy region.

We wish to thank Dr. G. Tungate for sending us the experimental data prior to the publication. We are grateful to Professor M. Kawai for stimulating discussions. This paper was financially supported by Grant-in Aid for Scientific Research. The financial supports are also offered by Research Center of Nuclear Physics, Osaka University and Institute for Nuclear Study, University of Tokyo for performing the computer work. The computer of Kyushu University in addition to those of the above institutes are utilized. One of the authors (Y.S.) also thanks the Japan Society for the Promotion of Science for the financial support.

Appendix Full expressions of analyzing powers by the invariant amplitudes

1. Analyzing powers in elastic scattering of spin 3/2 particles by 0^+ targets

The analyzing power T_{KQ} is given by

$$T_{KQ} = \mathrm{Tr}(M\tau_{KQ}M^+)/N \tag{A1}$$

with

$$N = \mathrm{Tr}(MM^+) .$$

Since the matrix elements of M, A-H, are given by the new invariant amplitudes U-$T_{3\beta}$ as is seen in eqs. (4.9), the analyzing power T_{KQ} is also expressed in terms of these amplitudes by the straightforward application of (4.9) to (A1).

$$iT_{11} = \frac{2\sqrt{6}}{\sqrt{5}N}\,\mathrm{Im}\Big\{\frac{1}{\sqrt{3}}US^* + \frac{2}{5\sqrt{3}}ST_{2\alpha}^* + \frac{2}{5}ST_{2\beta}^* \tag{A2}$$

$$+ \frac{1}{4}T_{2\alpha}T_{3\alpha}^*(\tan\theta + \frac{8}{5}\cot\theta) - \frac{1}{4\sqrt{3}}T_{2\beta}T_{3\alpha}^*(\tan\theta - \frac{4}{5}\cot\theta)$$

$$+ \frac{\sqrt{3}}{5}T_{2\alpha}T_{3\beta}^* + \frac{3}{5}T_{2\beta}T_{3\beta}^*\Big\} ,$$

$$T_{20} = \frac{2}{N}\,\mathrm{Re}\Big\{UT_{2\alpha}^* - \frac{4}{25}|S|^2 - \frac{3}{5}ST_{2\alpha}^*\tan\theta + \frac{\sqrt{3}}{5}ST_{2\beta}^*\tan\theta \tag{A3}$$

$$+ \frac{8\sqrt{3}}{25}ST_{3\alpha}^*\cot\theta + \frac{12}{25}ST_{3\beta}^* - \frac{2\sqrt{3}}{5}T_{2\alpha}T_{3\alpha}^* - \frac{3}{5}T_{2\beta}T_{3\alpha}^*$$

$$- \frac{3}{5}T_{2\alpha}T_{3\beta}^*\tan\theta + \frac{\sqrt{3}}{5}T_{2\beta}T_{3\beta}^*\tan\theta - \frac{12}{25}|T_{3\alpha}|^2\cot^2\theta$$

$$+ \frac{16}{25}|T_{3\beta}|^2 - \frac{12\sqrt{3}}{25}T_{3\alpha}T_{3\beta}^*\cot\theta\Big\} ,$$

$$T_{21} = \frac{2\sqrt{2}}{N}\,\mathrm{Re}\{-\frac{\sqrt{3}}{4}UT_{2\alpha}^{*}\tan\theta + \frac{1}{4}UT_{2\beta}^{*}\tan\theta - \frac{\sqrt{3}}{5}ST_{2\alpha}^{*} + \frac{1}{5}ST_{2\beta}^{*} \tag{A4}$$

$$- \frac{1}{5}ST_{3\alpha}^{*} - \frac{2}{5}T_{2\alpha}T_{3\alpha}^{*}\cot\theta - \frac{\sqrt{3}}{5}T_{2\beta}T_{3\alpha}^{*}\cot\theta - \frac{\sqrt{3}}{5}T_{2\alpha}T_{3\beta}^{*}$$

$$+ \frac{1}{5}T_{2\beta}T_{3\beta}^{*} + \frac{\sqrt{3}}{5}|T_{3\alpha}|^{2}\cot\theta + \frac{4}{5}T_{3\alpha}T_{3\beta}^{*}\} \ .$$

$$T_{T_{20}} \equiv -\frac{1}{2}(T_{20} + \sqrt{6}T_{22})$$

$$= -\frac{1}{N}\,\mathrm{Re}\{UT_{2\alpha}^{*} + \sqrt{3}UT_{2\beta}^{*} - \frac{16}{25}|S|^{2} + \frac{12\sqrt{3}}{25}ST_{3\alpha}^{*}\cot\theta + \frac{48}{25}ST_{3\beta}^{*}$$

$$+ \frac{12}{25}|T_{3\alpha}|^{2}\cot^{2}\theta + \frac{64}{25}|T_{3\beta}|^{2} + \frac{32\sqrt{3}}{25}T_{3\alpha}T_{3\beta}^{*}\cot\theta\} \ , \tag{A5}$$

$$iT_{31} = \frac{4}{\sqrt{5}N}\,\mathrm{Im}\{UT_{3\alpha}^{*}\cot\theta + \frac{\sqrt{3}}{2}UT_{3\beta}^{*} - \frac{\sqrt{3}}{5}ST_{2\alpha}^{*} - \frac{1}{10}ST_{2\beta}^{*} - \frac{5}{8}T_{2\alpha}T_{2\beta}^{*}\tan\theta$$

$$- \frac{1}{2}ST_{3\alpha}^{*} - \frac{3}{8}T_{2\alpha}T_{3\alpha}^{*}(\tan\theta + \frac{8}{5}\cot\theta) + \frac{\sqrt{3}}{8}T_{2\beta}T_{3\alpha}^{*}(\tan\theta + \frac{16}{5}\cot\theta)$$

$$- \frac{3\sqrt{3}}{10}T_{2\alpha}T_{3\beta}^{*} + \frac{11}{10}T_{2\beta}T_{3\beta}^{*} + \frac{1}{2}T_{3\alpha}T_{3\beta}^{*}\} \ .$$

$$iT_{32} = \frac{\sqrt{2}}{N}\,\mathrm{Im}\{-UT_{3\alpha}^{*} + \frac{\sqrt{3}}{5}ST_{2\alpha}^{*}\tan\theta - \frac{1}{5}ST_{2\beta}^{*}\tan\theta - T_{2\alpha}T_{2\beta}^{*} \tag{A6}$$

$$- \frac{4}{5}ST_{3\alpha}^{*}\cot\theta + \frac{3}{5}T_{2\alpha}T_{3\alpha}^{*} - \frac{\sqrt{3}}{5}T_{2\beta}T_{3\alpha}^{*} + \frac{4\sqrt{3}}{5}T_{2\alpha}T_{3\beta}^{*}\tan\theta$$

$$- \frac{4}{5}T_{2\beta}T_{3\beta}^{*}\tan\theta + \frac{4}{5}T_{3\alpha}T_{3\beta}^{*}\cot\theta\} \ ,$$

$$T_{T_{30}} \equiv -\frac{1}{2}(\sqrt{3}iT_{31} + \sqrt{5}iT_{33})$$

$$= \frac{1}{\sqrt{5}N}\,\mathrm{Im}\Big[-2\sqrt{3}UT_{3\alpha}^{*}\cot\theta - 8UT_{3\beta}^{*} + \frac{6}{5}ST_{2\alpha}^{*} + \frac{6\sqrt{3}}{5}ST_{2\beta}^{*} \qquad \text{(A7)}$$

$$+ 2\sqrt{3}T_{2\alpha}T_{3\alpha}^{*}(\tan\theta + \frac{3}{5}\cot\theta) - 2T_{2\beta}T_{3\alpha}^{*}(\tan\theta + \frac{11}{5}\cot\theta)$$

$$- \frac{16}{5}T_{2\alpha}T_{3\beta}^{*} - \frac{16\sqrt{3}}{5}T_{2\beta}T_{3\beta}^{*}\Big] .$$

The approximate formulae (4.11) are derived from the above by neglecting of the terms which includes $T_{3\alpha}$ and $T_{3\beta}$ but not U.

2. Scattering amplitudes and analyzing powers by the invariant amplitudes in the inelastic scattering to the $1/2^{-}$ excited state of ^{7}Li

The scattering matrix M of the inelastic scattering to the $1/2^{-}$ excited state of ^{7}Li is given by designating the row and column by the z-component of ^{7}Li spin in the initial and final states,

$$M = \begin{pmatrix} A & B & C & D \\ -D & C & -B & A \end{pmatrix} . \qquad \text{(A8)}$$

The matrix elements A~D are expressed in terms of the invariant amplitude $F_{K'K}$. Defining the new amplitudes analogously to (4.8),

$$S \equiv F_{11}\sin\theta , \qquad \text{(A9)}$$

$$T_{2\alpha} \equiv (\sqrt{6}F_{20}\cos\theta + F_{21})\sin\theta \ ,$$

$$T_{2\beta} \equiv \frac{1}{2\sqrt{2}}F_{20}(3\cos^2\theta - 1) + \sqrt{\frac{1}{3}}F_{21}\cos\theta + \frac{1}{\sqrt{2}}F_{22} \ ,$$

$$T_{2\gamma} \equiv \sqrt{\frac{3}{8}}F_{20}\sin^2\theta \ ,$$

we get

$$A = \frac{1}{4}(\sqrt{3}S - T_{2\alpha}) \ , \qquad \text{(A10)}$$

$$B = T_{2\beta} \ ,$$

$$C = \frac{1}{4}(S + \sqrt{3}T_{2\alpha}) \ ,$$

$$D = T_{2\gamma} \ .$$

The cross section σ is given by

$$\sigma = \left(\frac{k_f}{k_i}\right)\frac{N}{4}$$

and the analyzing powers by

$$iT_{11} = \frac{1}{\sqrt{10}N}\,\mathrm{Im}\{ST_{2\beta}^{*} + \sqrt{3}ST_{2\gamma}^{*} - 3\sqrt{3}T_{2\alpha}T_{2\beta}^{*} + 3T_{2\alpha}T_{2\gamma}^{*}\} \ ,$$

$$T_{20} = \frac{1}{N}\{\frac{1}{4}|S|^2 - \frac{\sqrt{3}}{2}\mathrm{Re}(ST_{2\alpha}^{*}) - \frac{1}{4}|T_{2\alpha}|^2 - 2|T_{2\beta}|^2 + 2|T_{2\gamma}|^2\} \ ,$$

$$T_{21} = \frac{1}{\sqrt{2}N} \mathrm{Re}\{-\sqrt{3}ST_{2\beta}^{*} + ST_{2\gamma}^{*} + T_{2\alpha}T_{2\beta}^{*} + \sqrt{3}T_{2\alpha}T_{2\gamma}^{*}\} ,$$

$$T_{20} = -\frac{1}{2N}\{|S|^2 - |T_{2\alpha}|^2 - 2|T_{2\beta}|^2 + 2|T_{2\gamma}|^2 + 4\sqrt{3}\mathrm{Re}(T_{2\beta}T_{2\gamma}^{*})\} ,$$

$$iT_{31} = \frac{1}{\sqrt{5}N} \mathrm{Im}\{2\sqrt{3}ST_{2\beta}^{*} + ST_{2\gamma}^{*} + 2T_{2\alpha}T_{2\beta}^{*} + \sqrt{3}T_{2\alpha}T_{2\gamma}^{*}\} ,$$

$$iT_{32} = \frac{1}{N} \mathrm{Im}\{-\frac{1}{\sqrt{2}}ST_{2\alpha}^{*} + 2\sqrt{2}T_{2\beta}T_{2\gamma}^{*}\} ,$$

$$T_{30} = -\frac{1}{\sqrt{5}N} \mathrm{Im}\{3ST_{2\beta}^{*} + 3\sqrt{3}ST_{2\gamma}^{*} + \sqrt{3}T_{2\alpha}T_{2\beta}^{*} - T_{2\alpha}T_{2\gamma}^{*}\} ,$$

where

$$N = 2\{\tfrac{1}{4}|S|^2 + \tfrac{1}{4}|T_{2\alpha}|^2 + |T_{2\beta}|^2 + |T_{2\gamma}|^2\}.$$

References

1) W. Weiss, P. Egelhof, K. D. Hildenbrand, D. Kassen, M. Makowska-Rzeszutko, D. Fick, H. Ebinghaus, E. Steffens, A. Amakawa and K.-I. Kubo, Phys. Lett. 61B (1976) 237

2) E. Steffens, Proc. Fifth Int. Symp. on Polar. Phenom. in Nucl. Phys. Santa Fe 1980, ed. G. G. Ohlsen, R. E. Brown, N. Jarmie, W. W. McNaughton and G. M. Hale (1981) p. 1001

3) Z. Moroz, P. Zupranski, R. Böttger, P. Egelhof, K.-H. Möbius, G. Tungate, E. Steffens, W. Dreves, I. Koenig and D. Fick, Nucl. Phys. A381 (1982) 294

4) Z. Moroz, K. Rusek, P. Egelhof, S. Kossionides, K.-H. Möbius, G. Tungate, E. Steffens, G. Grawert, I. Koenig and D. Fick, Nucl. Phys. A498 (1984) 498

5) Z. Moroz, Proc. Sixth Int. Symp. on Polar. Phenom. in Nucl. Phys., Osaka 1985, ed. M. Kondo, S. Kobayashi, M. Tanifuji, T. Yamazaki, K.-I. Kubo and N. Onishi, J. Phys. Soc. Jpn. 55 (1986) Suppl. p. 221

6) H. Ohnishi, M. Tanifuji and H. Noya, Phys. Lett. 103B (1981) 83

7) D. Mukhopadhyay, G. Grawert, D. Fick and Z. Moroz, Phys. Lett. 104B (1981) 361; D. Mukhopadhyay and G. Grawert, Nucl. Phys. A385 (1982) 133

8) J. Cook and R. J. Philpott, Nucl. Phys. A385 (1982) 157

9) H. Nishioka, R. C. Johnson, J. A. Tostevin and K.-I. Kubo, Phys. Rev. Lett. 48 (1982) 1795

10) H. Ohnishi, M. Tanifuji, M. Kamimura and M. Yahiro, Phys. Lett. 118B (1982) 16

11) H. Nishioka, J. A. Tostevin, R. C. Johnson and K.-I. Kubo, Nucl. Phys. A415 (1984) 230

12) H. Ohnishi, M. Tanifuji, M. Kamimura, Y. Sakuragi and M. Yahiro, Nucl. Phys. A415 (1984) 271

13) G. Grawert and D. Mukhopadhyay, Nucl. Phys. A415 (1984) 304

14) G. Windham, H. Nishioka, J. A. Tostevin and R. C. Johnson, Phys. Lett. 138B (1984) 253

15) H. Nishioka and R. C. Johnson, Phys. Rev. Lett. 53 (1984) 1881; Nucl. Phys. A440 (1985) 557

16) Y. Sakuragi, M. Kamimura, M. Yahiro and M. Tanifuji, Phys. Lett. 153B (1985) 372

17) M. Kamimura, Y. Sakuragi, M. Yahiro and M. Tanifuji, Proc. Sixth Int. Symp. on Polar. Phenom. in Nucl. Phys., Osaka 1985, ed. M. Kondo, S. Kobayashi, M. Tanifuji, T. Yamazaki, K.-I. Kubo and N. Onishi, J. Phys. Soc. Jpn., 55 (1986) Suppl. p. 205

18) Y. Sakuragi, M. Kamimura, M. Yahiro and M. Tanifuji, Proc. Sixth Int. Symp. on Polar. Phenom. in Nucl. Phys., Osaka 1985, ed. M. Kondo, S. Kobayashi, M. Tanifuji, T. Yamazaki, K.-I. Kubo and N. Onishi, J. Phys. Soc. Jpn., 55 (1986) Suppl. p. 770

19) M. Kamimura, Y. Sakuragi, M. Yahiro and M. Tanifuji, Proc. Sixth Int. Symp. on Polar. Phenom. in Nucl. Phys., Osaka 1985, ed. M. Kondo, S. Kobayashi, M. Tanifuji, T. Yamazaki, K.-I. Kubo and N. Onishi, J. Phys. Soc. Jpn., 55 (1986) Suppl. p. 768

20) Y. Sakuragi, M. Kamimura, M. Yahiro and M. Tanifuji, Phys. Lett. (1986) in press

21) K.-H. Möbius, Z. Phys. A310 (1983) 159

22) M. Tanifuji and K. Yazaki, Prog. Theor. Phys. 40 (1968) 1023

23) Y. Sakuragi, M. Yahiro and M. Kamimura, Prog. Theor. Phys. 70 (1983) 1047

24) G. R. Satchler and W. G. Love, Phys. Rep. 55 (1979) 183

25) M. Kamimura, Y. Iseri, Y. Sakuragi, M. Yahiro and M. Nakano, Proc. Fourth Int. Conf. on Clustering Aspects of Nuclear Structure, Chester 1984, ed. J. S. Lilley and M. A. Nagarajan, (D. Reidel Publishing company) p. 181

26) F. Ajzenberg-Selove, Nucl. Phys. A320 (1979) 1

27) R. J. Spiger and T. A. Tombrello, Phys. Rev. 163 (1967 964

28) L. R. Suelzle, M. R. Yearian and Hall Crannell, Phys. Rev. 162 (1967) 992;

G. J. C. van Niftrik, L. Lapikas, H. deVries and G. Box, Nucl. Phys. A174 (1971) 173

29) D. P. Stanley, F. Petrovich and P. Schwandt, Phys. Rev. C22 (1980) 1357

30) D. Fick, private communication

31) C. M. Perey and F. G. Perey, Atomic Data and Nucl. Data Tables 17 (1976) 1

32) J. R. Ficenec, L. A. Fajardo and W. P. Trower, Phys. Lett. 42B (1972) 213

33) G. Tungate, private communication

34) R. A. Hardekopf, R. F. Haglund, Jr., G. G. Ohlsen, W. J. Thompson and L. R. Veeser, Phys. Rev. C21 (1980) 906

35) G. R. Satchler, in Direct Nuclear Reacions (Clarendon Press, Oxford; Oxford University Press, New York, 1983) p. 395

36) M. Tanifuji, M. Kamimura and Y. Sakuragi, Proc. Sixth Int. Symp. on Polar. Phenom. in Nucl. Phys., Osaka 1985, ed. M. Kondo, S. Kobayashi, M. Tanifuji, T. Yamazaki, K.-I. Kubo and N. Onishi, J. Phys. Soc. Jpn. 55 (1986) Suppl. p.198

37) D. J. Hooton and R. C. Johnson, Nucl. Phys. A175 (1971) 583

38) H. Ohnishi and M. Tanifuji, to be published

Table Caption

Table 1. Parameters of optical potentials for α-Sn and t-Sn in the cluster-folding interaction. The sets A1 and A2 are for the shallow α-Sn potential and the deep one, respectively[31]. The sets T1-T4 are for the t-Sn potential[31,34], where the spin-orbit potential is included in T2 and T4. Other notations are as usual.

Figure Captions

Fig. 1. Incident energies against Coulomb barrier. Center-of-mass incident energies for scattering of ^{7}Li by ^{12}C at E_{lab}=20 MeV, by ^{58}Ni at E_{lab} =14 and 20 MeV and by ^{120}Sn at E_{lab}=44 MeV are shown in comparison with the Coulomb barrier.

Fig. 2. Coordinates for double-folding calculations. P and T represent the projectile and the target nucleus, respectively.

Fig. 3. Comparison between cluster-folding calculations and double-folding ones in ^{7}Li-^{58}Ni scattering at E_{lab}=20 MeV. The cross section and the vector and second-rank tensor analyzing powers by the four-channel CC calculation are shown for the elastic scattering (a) and for the inelastic scattering to the first $1/2^{-}$ excited state of ^{7}Li (b). The calculated quantities by the CF interaction and by the DF one are described by the dashed lines and the solid lines, respectively. They are compared with each other and with the experimental data[3].

Fig. 4. Comparison between cluster-folding calculations and double-folding ones in ^{7}Li-^{120}Sn scattering at E_{lab}=44 MeV. The cross section and the vector, second-rank tensor and third-rank tensor analyzing powers by the four-channel CC calculation are shown for the elastic scattering and the inelastic one to the first $1/2^{-}$ excited state of ^{7}Li. The calculated quantities by the CF interaction with the A1-T1 input combination and those by the DF interaction are described by the dashed lines and the solid ones, respectively. They are compared with each other and with the experimental data[33].

Fig. 5. Effects of spin-orbit interactions in the cluster-folding calculation for the scattering of ^{7}Li by ^{120}Sn at E_{lab}=44 MeV. The calculations by two combinations of the input potentials are compared with each other and with the data[33], where the triton-target potential with a spin-orbit potential (T2) and the one without (T3) are combined to the shallow α-target potential (A1). The calculations are performed in the CC frame with the four channels and are shown for the cross section and the vector, second-rank tensor and third-rank tensor analyzing powers for the elastic scattering and the inelastic one to the first $1/2^{-}$ excited state of ^{7}Li. The solid and dashed lines denote the combination A1-T2 and A1-T3, respectively.

Fig. 6. Demonstration of effects of spin-orbit interactions in ^{7}Li-^{120}Sn elastic scattering at E_{lab}=44 MeV. The dotted line is for the single-channel calculation by the central plus spin-orbit interaction, the dashed one for the four-channel calculation by the

central plus tensor interaction and the solid one for the four-channel calculation which contains both spin-dependent interactions. The interaction is based on the A1-T2 CF one.

Fig. 7. Form factors of folding potentials for ^{7}Li from ^{120}Sn. The form factors of the diagonal potentials are compared between the shallow CF interaction (dashed lines), the deep CF one (solid lines) and the DF one (dotted lines) in the range 5-13 fm of the projectile-target relative distance. The strong absorption radius is shown by R_s.

Fig. 8. Effects of projectile virtual excitations on cross sections and vector and second- and third-rank tensor analyzing powers in the scattering of ^{7}Li by ^{120}Sn at E_{lab}=44 MeV. The effects of the projectile virtual excitation are shown for the observables in both of the elastic and inelastic scattering. The dash-dotted lines, the dotted ones, the dashed ones and the solid ones are for the single-channel calculation, the two-channel one, the three-channel one and the four-channel one, respectively. The interaction is the A1-T1 CF one.

Fig. 9. Effects of spin-orbit interactions and projectile virtual excitations on $|U|$, $|S|$, $|T_{2\alpha}|$, $|T_{2\beta}|$, $|T_{3\alpha}|$ and $|T_{3\beta}|$ in ^{7}Li-^{120}Sn scattering at E_{lab}=44 MeV. The LS effects in the elastic-scattering amplitudes are shown in the upper figures (a) and the projectile-excitation effects in the lower figures (b). The calculations in (a) are in the four-channel CC frame where the solid lines and dotted ones are for the A1-T2 CF interaction and A1-T3 CF one, respectively. In (b), the A1-T3 CF interaction is used, where the solid lines and the dashed lines are for the four-channel calculation and the single-channel one, respectively.

Fig. 10. Comparison between the CF calculation and the DF one in $|U|$, $|S|$, $|T_{2\alpha}|$, $|T_{2\beta}|$, $|T_{3\alpha}|$ and $|T_{3\beta}|$ in ^{7}Li-^{120}Sn scattering at E_{lab}=44 MeV. The calculation is for the elastic scattering and takes account of the four channels. The solid lines and the dashed lines are for the DF interaction and for the A1-T1 CF one, respectively.

Fig. 11. Dependences of invariant amplitudes on the strength of the second-rank tensor interactions in ^{7}Li-^{120}Sn scattering at E_{lab}=44 MeV. The magnitudes of U, S, $T_{2\alpha}$, $T_{2\beta}$, $T_{3\alpha}$ and $T_{3\beta}$ in the elastic scattering are shown for the A1-T3 CF interaction (dash-dotted lines) and for the modified interaction (solid lines) where the strength of the second-rank tensor interaction is reduced to one half of that of the original interaction. For these lines the fourth- and sixth-rank tensor interactions are neglected. The dotted lines are for the original A1-T3 interaction. All calculations take account of the four channels.

Fig. 12. Examinations of approximations for analyzing powers in ^{7}Li-^{120}Sn scattering at E_{lab}=44 MeV. The calculations by approximations I (dashed lines) and II (dotted lines) for the vector analyzing power and the second- and third-rank tensor ones in the elastic scattering are compared with each other and with the exact calculation (solid lines). In the second-rank tensor analyzing powers, the approximation I cannot be resolved from the exact in the figure. For the third-rank tensor analyzing power, the single-channel calculation is additionally displayed. Others are by the four-channel calculation. The A1-T2 CF interaction is used.

Fig. 13. Examination of the relationship between the tensor analyzing powers for ^{7}Li-^{120}Sn scattering at E_{lab}=44 MeV. The right-hand side of eq. (4.12) (dashed lines) is compared with the left-hand side calculated exactly (solid lines) for the A1-T2 CF interaction and the DF one in the elastic scattering. The calculation is performed in the four-channel frame.

Fig. 14. Examination of shape-effect formulae in ^{7}Li-^{120}Sn elastic scattering at E_{lab}=44 MeV. The solid lines for T_{20} and T_{21} are calculated by eqs. (4.14) and (4.15), respectively, by using the experimental data properly connected by the dotted line for $^{T}T_{20}$ in the right-hand sides of the equations. The data are from ref. 33).

Fig. 15. Dependences of cross section and analyzing powers on the strength of the second-rank tensor interactions in ^{7}Li-^{120}Sn scattering at E_{lab}=44 MeV. The cross section, the vector analyzing power and the second- and third-rank tensor analyzing powers in both of the elastic scattering and the inelastic one are shown for the A1-T3 CF interaction (dash-dotted lines) and for the modified interaction (solid lines) where the strength of the second-rank tensor interaction is reduced to one half of that of the original interaction. For these lines the fourth- and sixth tensor interactions are neglected and the calculations take account of the four channels.

Table 1

	V_0	r_0	a_0	W_v	r_w	a_w	V_{so}	r_{so}	a_{so}	r_c
A1	45.4	1.562	0.556	11.00	1.562	0.556				1.30
A2	218.6	1.373	0.553	29.87	1.373	0.553				1.34
T1	147.0	1.240	0.688	18.08	1.475	0.890	0.0			1.25
T2	151.5	1.200	0.660	14.50	1.600	1.00	8.00	1.10	0.80	1.30
T3	151.5	1.200	0.660	14.50	1.600	1.00	0.0			1.30
T4	147.0	1.240	0.688	18.08	1.475	0.890	8.00	1.10	0.80	1.25

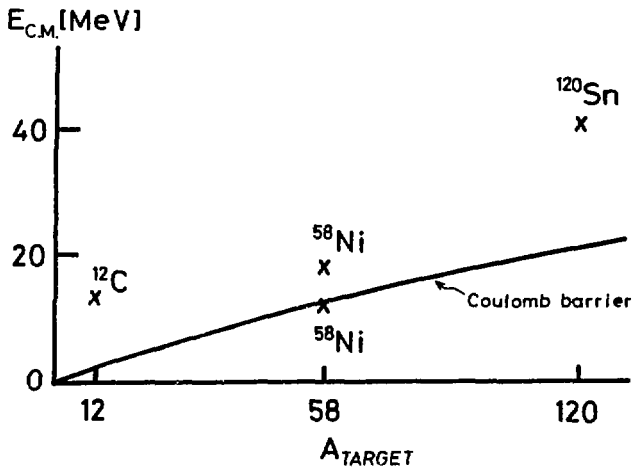
E C.M. [MeV]
40
20
0
12
58
120
A TARGET
120Sn
58Ni
12C
58Ni
Coulomb barrier

Fig. 1

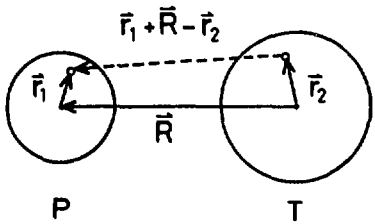

Fig. 2

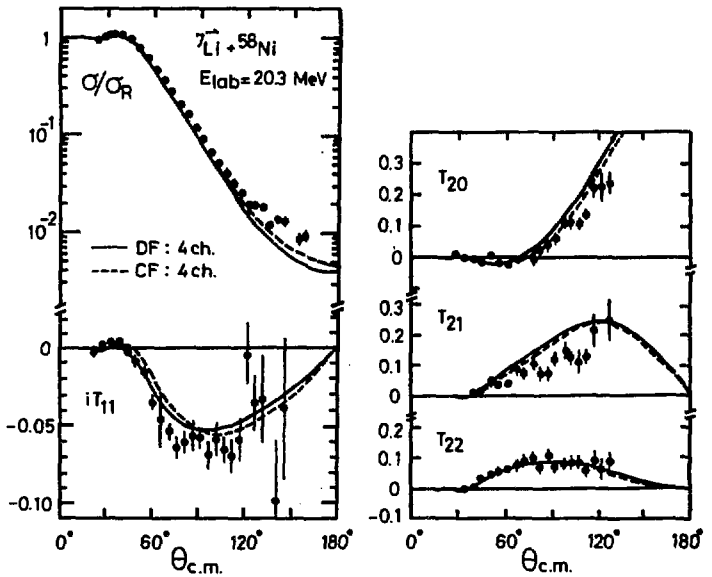
$\vec{^7Li}$ + ^{58}Ni
Elab=20.3 MeV
σ/σR
DF : 4ch.
CF : 4ch.
iT11
T20
T21
T22
θc.m.
θc.m.

Fig. 3a

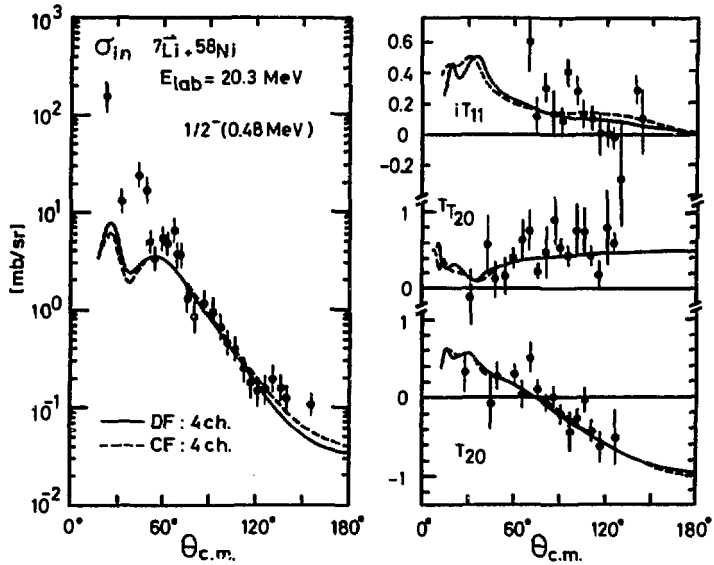
σ_{in} $^{7}\vec{Li}+^{58}Ni$
E_{lab}= 20.3 MeV
1/2⁻(0.48 MeV)
DF : 4ch.
CF : 4ch.
[mb/sr]
$\theta_{c.m.}$
iT_{11}
T_{T20}
T_{20}

Fig. 3b

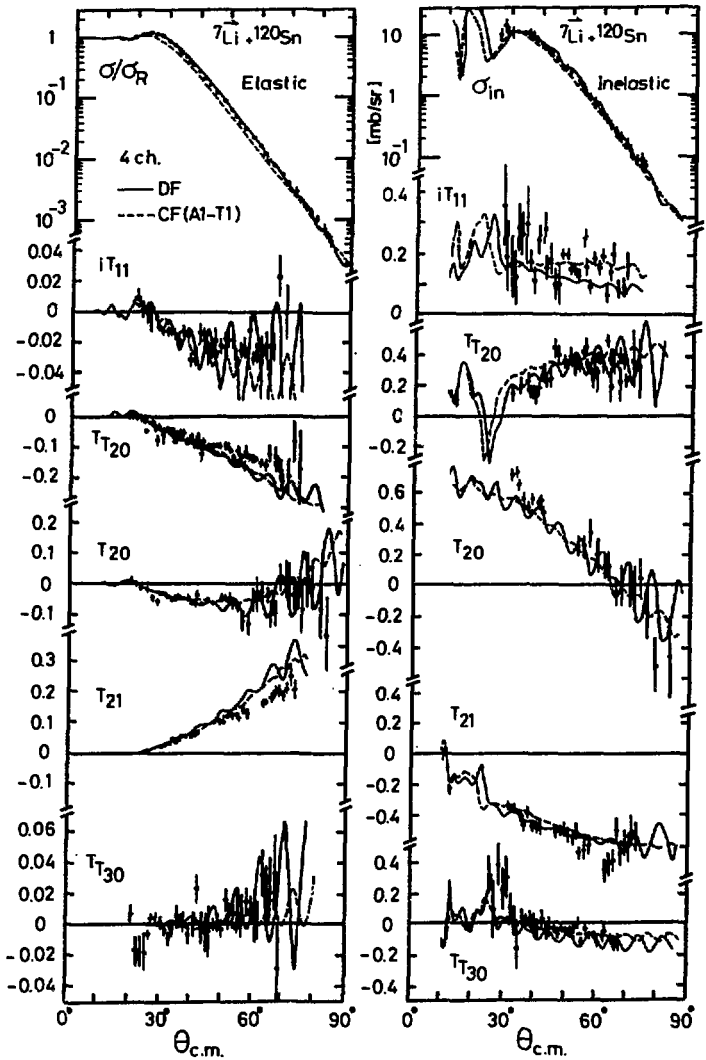
7Li + 120Sn
σ/σR
Elastic
4 ch.
DF
CF(A1-T1)
iT11
TT20
T20
T21
TT30
θc.m.
7Li + 120Sn
σin
Inelastic
[mb/sr]
iT11
TT20
T20
T21
TT30
θc.m.

Fig.4

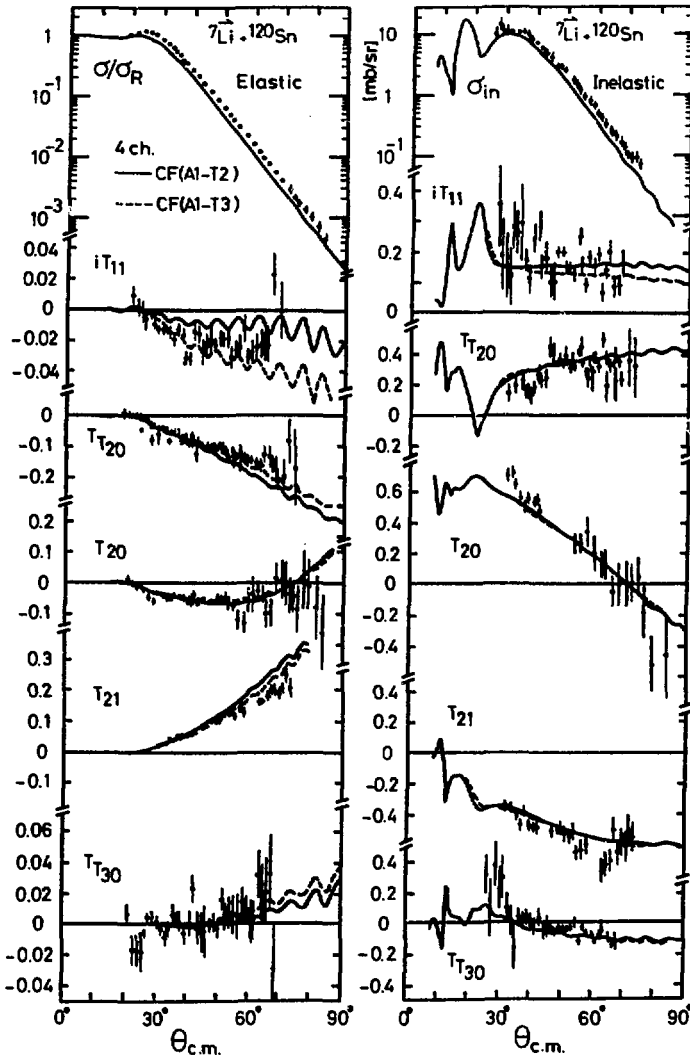
7Li + 120Sn
σ/σR
Elastic
4 ch.
CF(A1-T2)
CF(A1-T3)
iT11
TT20
T20
T21
TT30
7Li + 120Sn
σin
Inelastic
(mb/sr)
iT11
TT20
T20
T21
TT30
0°
30°
60°
90°
θc.m.
θc.m.

Fig. 5

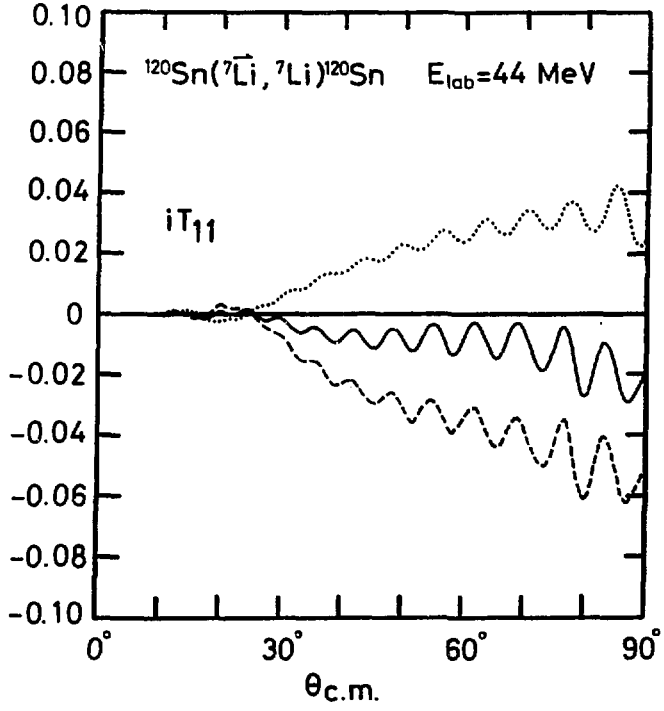
0.10
0.08
0.06
0.04
0.02
0
-0.02
-0.04
-0.06
-0.08
-0.10
$^{120}Sn(^{7}\vec{Li}, ^{7}Li)^{120}Sn$ E_{lab}=44 MeV
iT_{11}
0°
30°
60°
90°
$\theta_{c.m.}$

Fig. 6

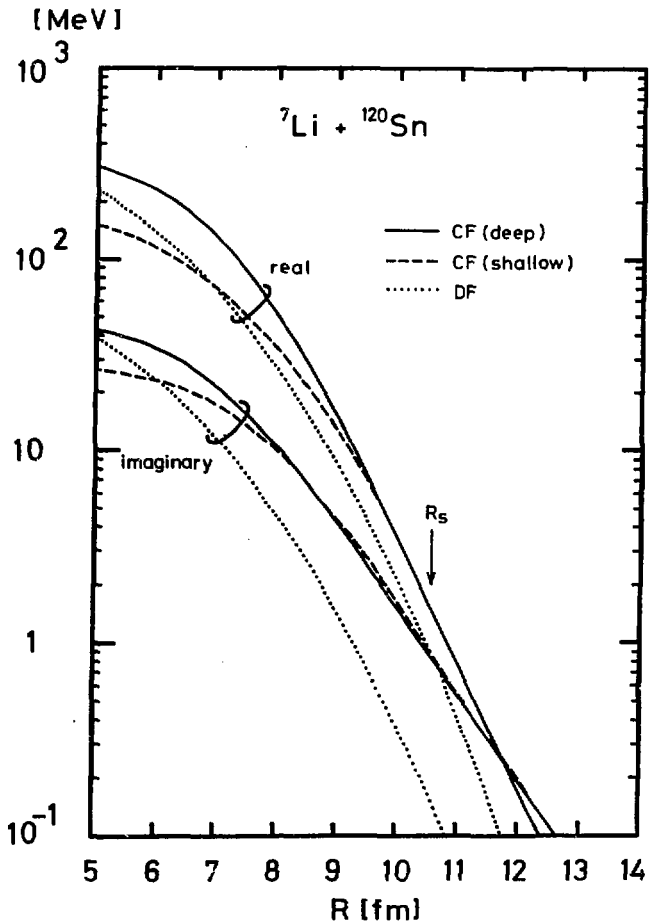
[MeV]
10 3
10 2
10
1
10 -1
7Li + 120Sn
CF (deep)
CF (shallow)
DF
real
imaginary
Rs
5 6 7 8 9 10 11 12 13 14
R [fm]

Fig. 7

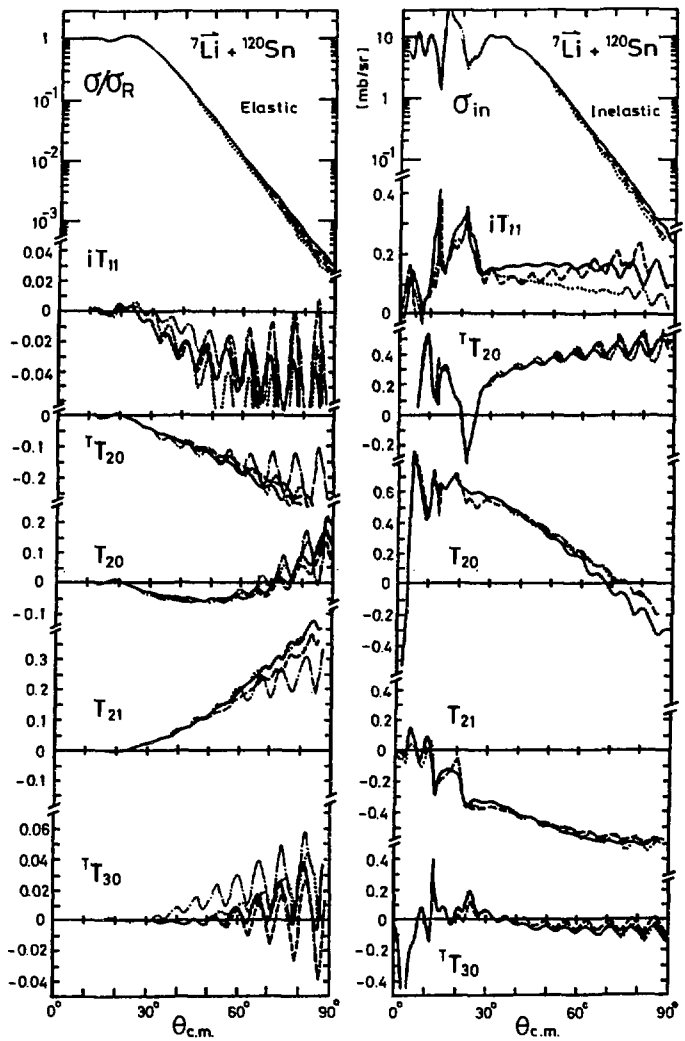
$^7\vec{Li}$ + ^{120}Sn
σ/σ_R
Elastic
iT11
T20
T20
T21
T30
(mb/sr)
σ_in
Inelastic
iT11
T20
T20
T21
T30
θc.m.
θc.m.

Fig. 8

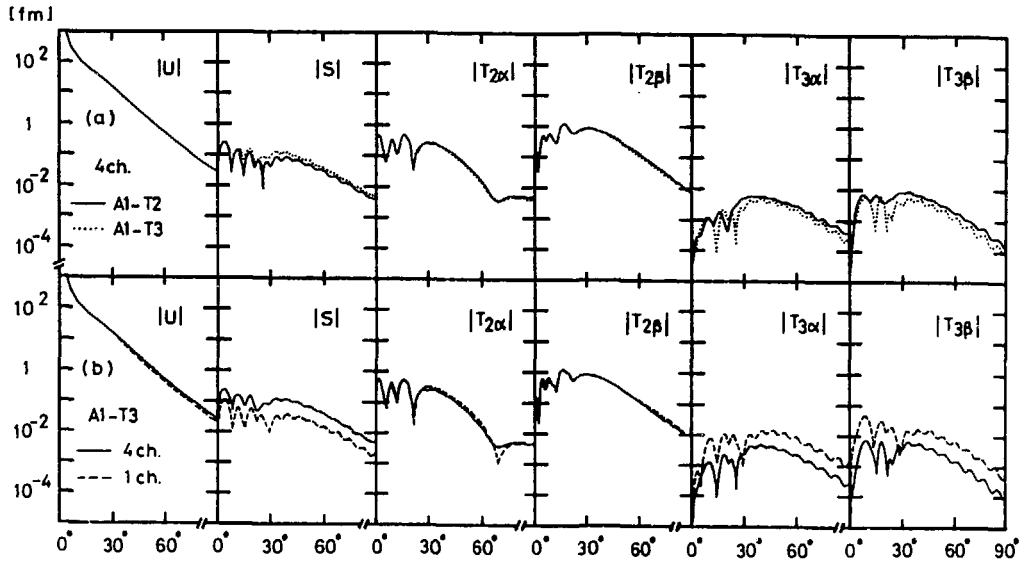
[fm]
|U|
|S|
|T2α|
|T2β|
|T3α|
|T3β|
(a)
4ch.
A1-T2
A1-T3
(b)
A1-T3
4ch.
1ch.
10^2
1
10^-2
10^-4
0°
30°
60°
90°

Fig. 9

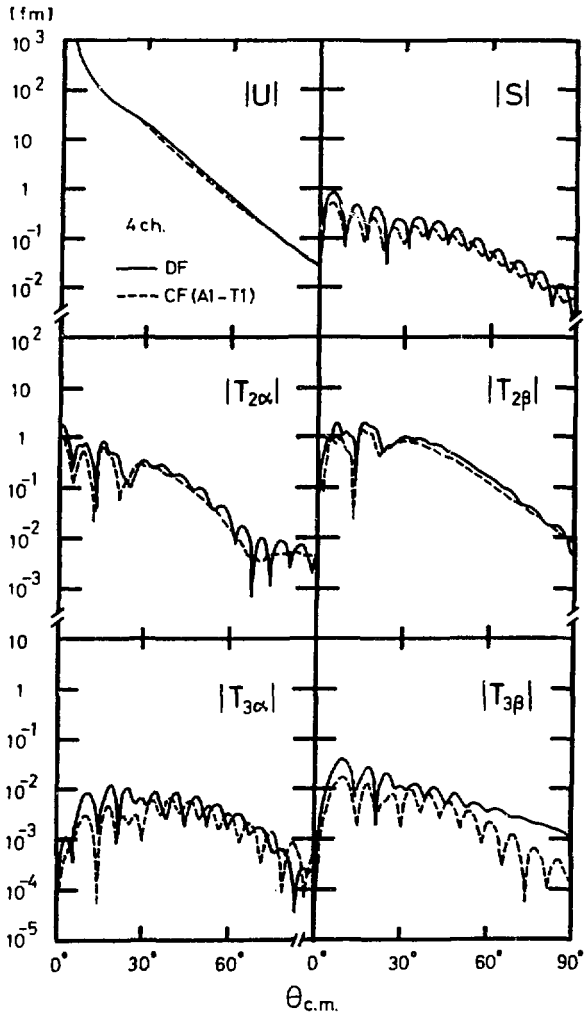

Fig. 10

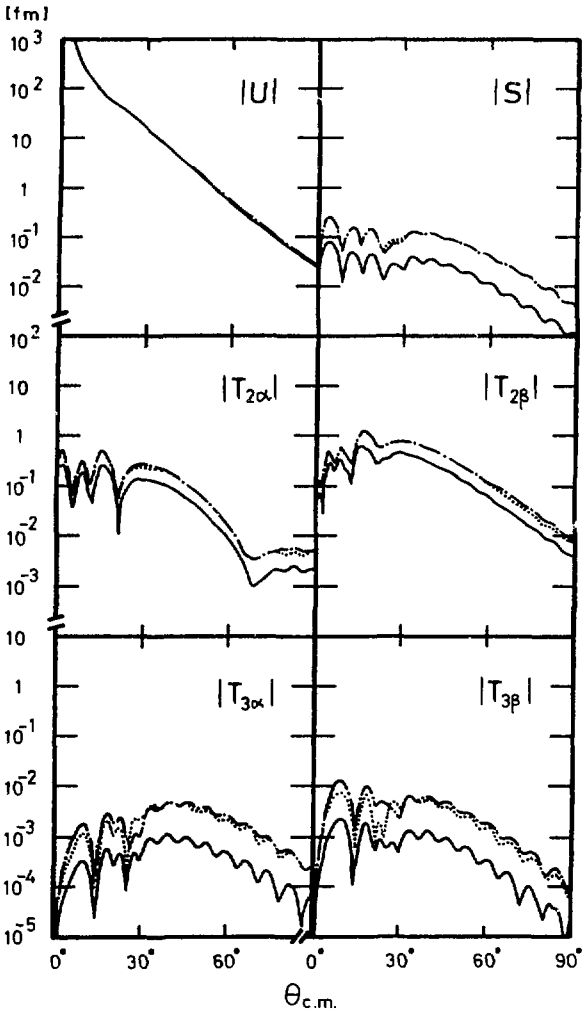

Fig. 11

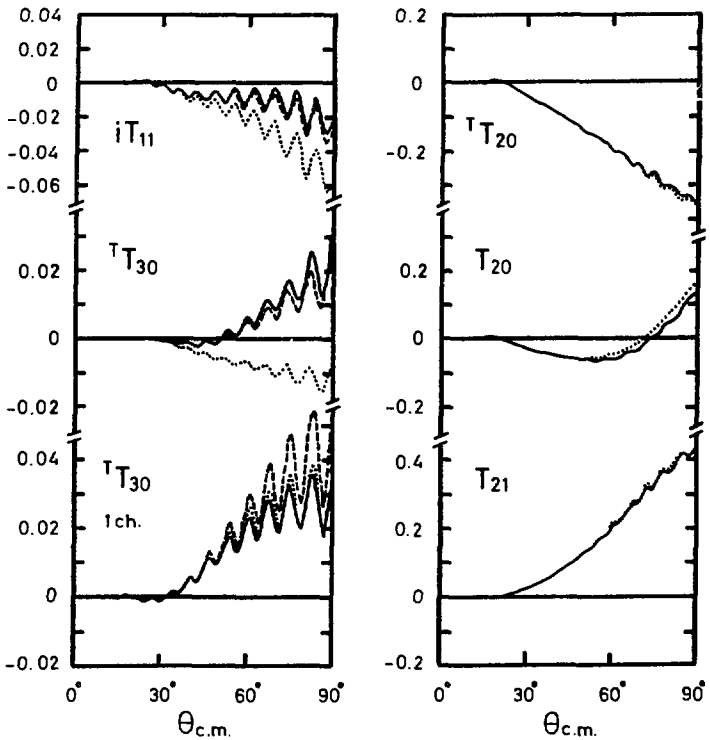
0.04
0.02
0
-0.02
-0.04
-0.06
iT11
TT30
0.02
0
-0.02
0.04
TT30
1ch.
0.02
0
-0.02
0°
30°
60°
90°
θc.m.
0.2
0
-0.2
TT20
T20
0.2
0
-0.2
0.4
T21
0.2
0
-0.2
0°
30°
60°
90°
θc.m.

Fig. 12

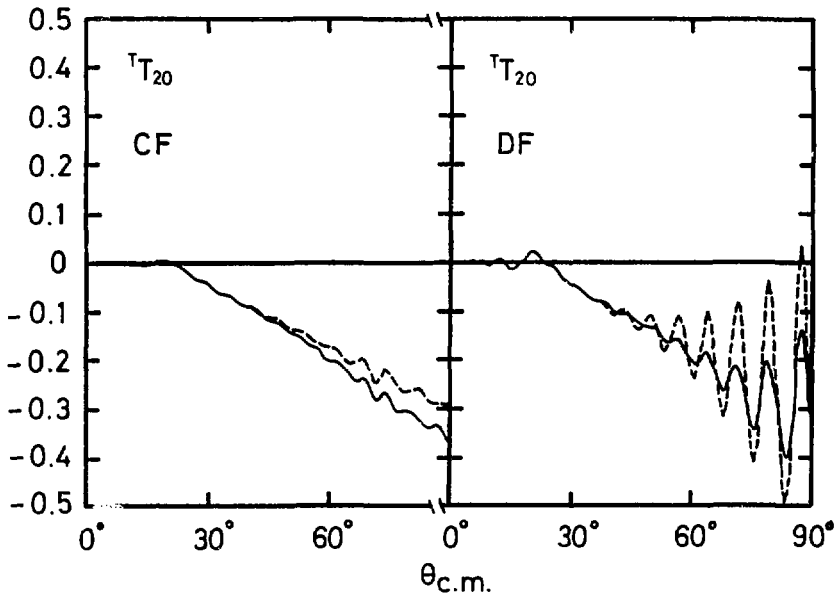
0.5
0.4
0.3
0.2
0.1
0
-0.1
-0.2
-0.3
-0.4
-0.5
$^{T}T_{20}$
CF
$^{T}T_{20}$
DF
0°
30°
60°
0°
30°
60°
90°
$\theta_{c.m.}$

Fig. 13

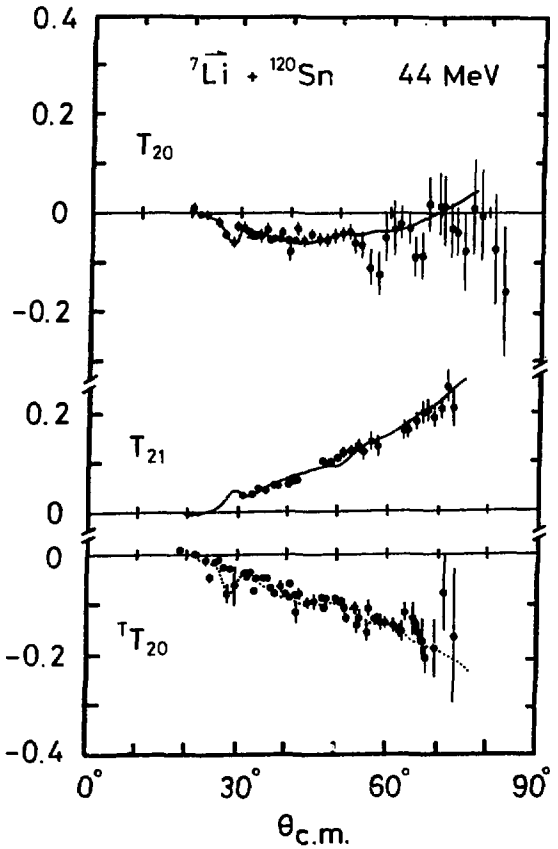
0.4
0.2
0
-0.2
$^7\vec{Li}$ + ^{120}Sn 44 MeV
T_{20}
0.2
0
T_{21}
0
-0.2
-0.4
$^TT_{20}$
0°
30°
60°
90°
$\theta_{c.m.}$

Fig. 14

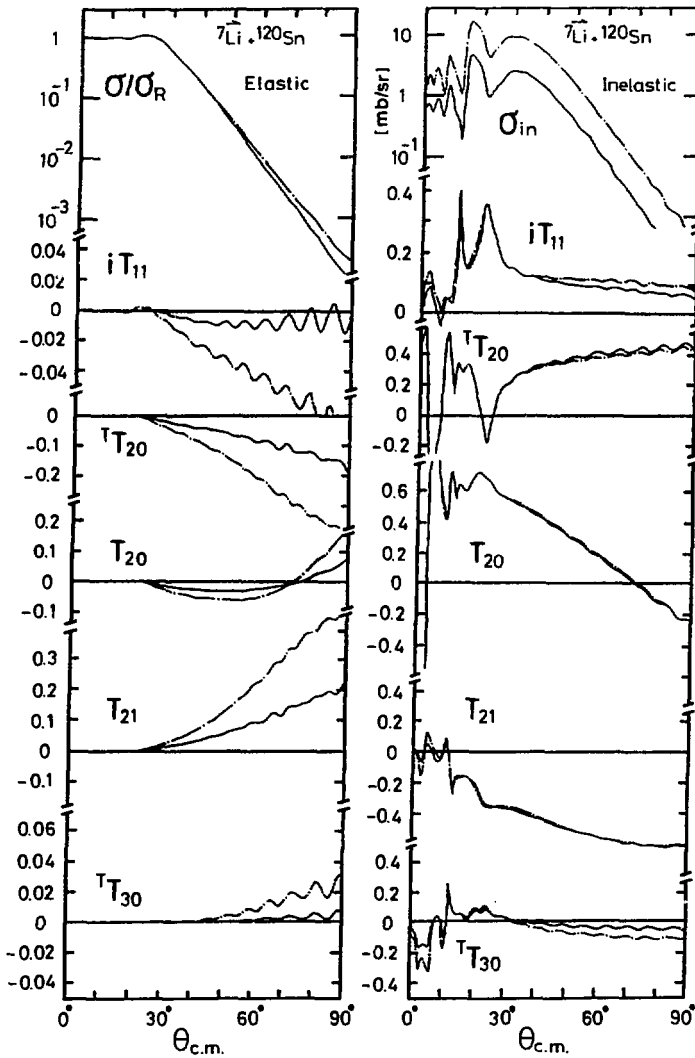
7Li + 120Sn
Elastic
σ/σR
iT11
tT20
T20
T21
tT30
θc.m.
7Li + 120Sn
Inelastic
[mb/sr]
σin
iT11
tT20
T20
T21
tT30
θc.m.

Fig. 15